Chapter

Dielectric Losses of Microwave Ceramics Based on Crystal Structure

Hitoshi Ohsato, Jobin Varghese and Heli Jantunen

Abstract

So far, many microwave dielectric materials have been investigated for a range of telecommunication applications. In dielectrics, the three main dielectric properties are quality factor (Q), dielectric constant and temperature coefficient of resonant frequency. Among these, the most essential dielectric property is Q. More specifically, Q is the inverse of the dielectric loss ($\tan\delta$); thus $Q = 1/\tan\delta$. There are two kinds of losses: those depending on crystal structure and losses due to external factors. The former is intrinsic losses such as ordering, symmetry, and phonon vibration. The latter is extrinsic losses due to factors such as grain size, defects, inclusions and distortion. In this chapter, the authors present the origin of dielectric losses based on the crystal structure. An ideal and well-proportional crystal structure constitutes a low loss material. Most dielectric materials are paraelectrics with inversion symmetry i and high symmetry. In general, it is believed that ordering gives rise to a high Q, on which many researchers are casting doubt. In the case of complex perovskites, the symmetry changes from cubic to trigonal. Ordering and symmetry should be compared with the structure. In this chapter, three essential conditions for the origin of high Q such as high symmetry, compositional ordering and compositional density are presented.

Keywords: microwave dielectrics, Q-factor, ordering, symmetry, indialite/cordierite, pseudo tungsten-bronze, complex perovskite

1. Introduction

Microwave and millimetre-wave dielectric materials [1–6] have been investigated for a wide range of telecommunication applications, such as mobile and smartphones, wireless local area network (LAN) modules and intelligent transport system (ITS). Millimetre-wave dielectric materials with high quality factor Q and low dielectric constant ε_r are required for the next 5G telecommunication applications used for noncondensed high data transfer on LAN/ personal area networks (PAN) and the higher frequency radar on autonomous cars.

In microwave dielectrics, there are three fundamental dielectric properties: quality factor (Q), dielectric constant (ε_r) and temperature coefficient of resonant frequency (TCf/τ_f) [1, 2, 6]. Microwave dielectrics have been used as the critical constituents of wireless communications [7–10], such as resonators, filters and temperature-stable capacitors with a near zero ppm/°C $TC\varepsilon_r$ (temperature

coefficient of the dielectric constant). Among the dielectric properties, the most essential property is Q, the inversion of the dielectric loss ($\tan\delta$); thus $Q = 1/\tan\delta$. The dielectric losses of microwave dielectrics should be small. So, most of the microwave dielectrics are paraelectrics with inversion symmetry i, while most of the electronic materials are ferroelectrics with spontaneous polarity showing substantial dielectric losses [11–13]. The microwave dielectrics attract attention as a high potential material, which have an over-well-proportional rigid crystal structure with symmetry. That is, the structure should be without electric defects, nondistortion and without strain.

Under the influence of an electric field, four types of polarisation mechanisms can occur in dielectric ceramics, that is, interfacial, dipolar, ionic and electronic. In general, the microwave dielectric properties such as ε_r and Q are mostly influenced by ionic or electronic polarisation. The dielectric polarisation generates the dielectric losses in the presence of an electromagnetic wave. When the frequency is increased to millimetre-wave values, the dielectric losses may be increased or decreased depending on the polarisation mechanism. There are two kinds of losses: those depending on crystal structure and losses due to external factors. It was believed that the intrinsic losses are due to the ordering/disordering, symmetry and phonon vibration, while extrinsic losses are due to factors such as grain size, defects, inclusions, density and distortion from stress.

In this chapter, the origins of high Q are discussed based on the intrinsic factors related to the crystal structure, such as symmetry, compositional ordering and compositional density. Although it has previously been believed that ordering based on the order-disorder phase transition brings high Q [14], the authors propose that it is primarily a high symmetry that leads to high Q [15]. The following focused studies relate to specific examples; indialite with high symmetry showing higher Q than cordierite with an ordered structure [16–18]; pseudo tungsten-bronze solid solutions without phase transition showing high Q based on the compositional ordering [19–21]; complex perovskite compounds with order-disorder transitions depending on density and grain size [22, 23] and complex perovskites with composition deviated from the stoichiometric depending on the compositional density showing a high Q [24–29].

2. Focused studies

2.1 Indialite/cordierite glass ceramics

2.1.1 Indialite Q-factor improved by Ni-substitution

Cordierite ($Mg_2Al_4Si_5O_{18}$) has two polymorphs: cordierite and indialite, as shown in **Figure 1(a)** and **(c)**, respectively [30, 31]. Cordierite is of low symmetry form: orthorhombic crystal system *Cccm* (No. 66), which has $Si_4Al_2O_{18}$ six-membered tetrahedron rings with ordered SiO_4 and AlO_4 tetrahedra as shown in **Figure 1(b)**. On the other hand, indialite is of high symmetry form: hexagonal crystal system *P6/mcc* (No. 192), which has disordered $Si_4Al_2O_{18}$ equilateral hexagonal rings as shown in **Figure 1(c)**.

Cordierite shows a lower ε_r of 6.19 which depends on the silicates and a near-zero *TCf* of −24 ppm/°C [32] as compared to other silicates as shown in **Figure 2(a)**. Based on these properties, Terada et al. carried out initiative research on these microwave dielectrics [16]. They reported an excellent *Qf* by substituting Ni for Mg as shown in **Figure 2(b)**. The *Qf* was improved from 40×10^3 GHz to 100×10^3 GHz by Ni substitution of $x = 0.1$ in $(Mg_{1-x}Ni_x)_2Al_4Si_5O_{18}$. The Ni substitution did not change the ε_r value

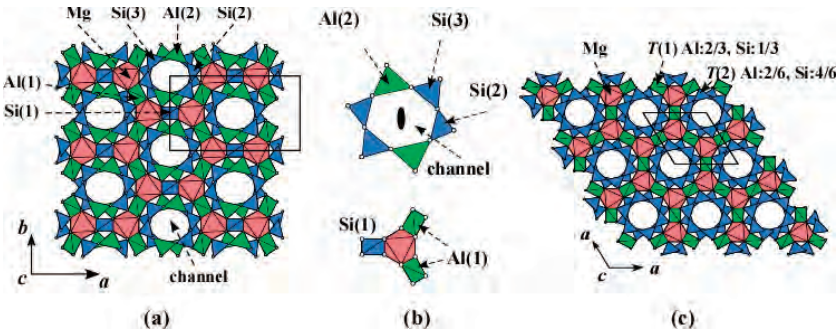

Figure 1.
Schematic representation of cordierite (a), six-membered tetrahedron ring with ordered SiO_4 and AlO_4 (b) and indialite (c).

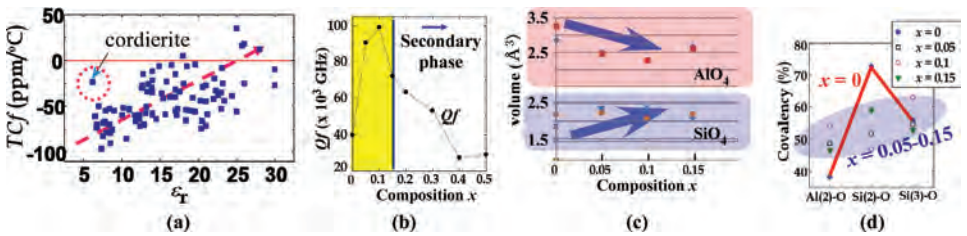

Figure 2.
Cordierite with near zero ppm/°C deviated from other compounds (a). Ni-substituted cordierite Qf (b), volume of AlO_4 and SiO_4 (c) and covalencies of Si-O and Al-O as a function of composition x (d).

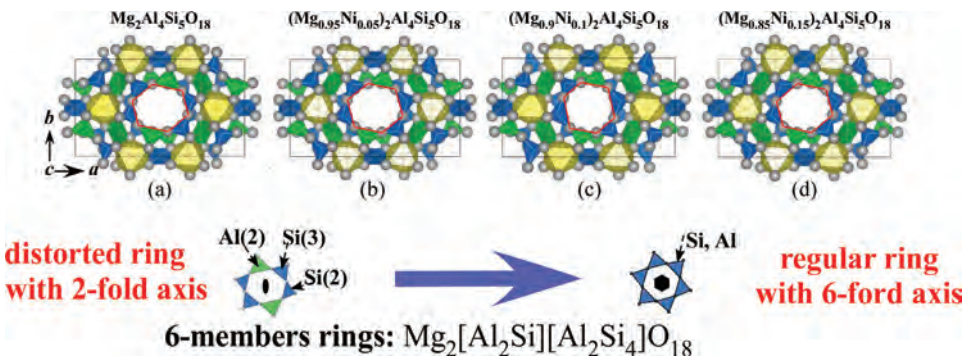

Figure 3.
Crystal structure of Ni-substituted cordierite: $(Mg_{1-x}Ni_x)_2Al_4Si_5O_{18}$ with composition x = 0 (a), 0.05 (b), 0.1 (c) and 0.15 (d).

considerably, but the *TCf* was degraded from −24 to −30 ppm/°C [16]. For $x > 0.1$, the properties were affected by the formation of the secondary phase of $NiAl_2O_4$.

Terada et al. also analysed the crystal structure by the Rietveld method [33] to clarify the origin of the improved *Qf* value. The X-ray powder diffraction (XRPD) pattern was obtained by a multi-detector system (MDS) [34] in the synchrotron radiation "Photon Factory" of the National Laboratory for High Energy Physics in Tsukuba, Japan. **Figure 3(a)–(d)** shows the crystal structures of Ni-substituted cordierite $(Mg_{1-x}Ni_x)_2Al_4Si_5O_{18}$ with $x = 0$, 0.05, 0.1 and 0.15. The crystal structure showed a tendency to deform to indialite with high symmetry on the hexagonal ring composed of corner-sharing of (Si, Al)O_4 tetrahedra in the *a*-*b* plane. Ni-substituted cordierite $(Mg_{1-x}Ni_x)_2Al_4Si_5O_{18}$ with composition $x = 0.1$

(**Figure 3(c)**) was obviously closer to equilateral hexagonal rings compared to ($Mg_{0.95}Ni_{0.05})_2Al_4Si_5O_{18}$ (**Figure 3(b)**) and $Mg_2Al_4Si_5O_{18}$ (**Figure 3(a)**).

The transformation from cordierite to indialite, represented by the ratio of disordering between the SiO_4 and AlO_4 tetrahedra, is based on the volumes and covalencies of the SiO_4 and AlO_4 tetrahedra [35]. The volume was calculated using atomic coordinates obtained by Rietveld crystal structural analysis as shown above. The covalency (f_c) of the cation-oxygen bond was estimated from the following equation [36].

$$f_c = as^M \tag{1}$$

The empirical constants a and M depending on the inner-shell electron number 10 are 0.54 v.u. and 1.64, respectively [37], where s is the bond length obtaining from the following equation:

$$s = (R/R1)^{-N} \tag{2}$$

where, R is defined as the bond length, and $R1$ and N are the measured parameter reliant on the cation site and each cation-anion pair, respectively.

Figure 2(c) and **(d)** depicts the calculated volume and covalency of SiO_4 and AlO_4 octahedra, respectively. These figures show the phase changing from cordierite to indialite as substitution of Ni in the Mg site. In the cordierite $Mg_2Al_4Si_5O_{18}$ (**Figure 1(a)**), Si/Al ions in the tetrahedra are ordered. Therefore, the volume and covalency of tetrahedra are different values, but the values are becoming similar to the substitution of Ni in the Mg site. This is due to the disordering of Si/Al ion phase transition in the cordierite (**Figure 1(a)**) to indialite (**Figure 1(c)**). In the indialite, the disordered $Si_4Al_2O_{18}$ equilateral hexagonal rings with 6-ford axis are the main framework as analysed by the Rietveld method as shown in **Figure 3(d)**. The improvement of *Qf* as shown in **Figure 2(b)** should be based on the disordering due to high symmetry instead of an ordering of SiO_4 and AlO_4 tetrahedra by order-disorder transition. It is one example of high symmetry bringing a higher Q than ordering by the order-disorder transition [18].

2.1.2 Indialite glass ceramics with high Q

As described in the previous section, the *Qf* value of indialite derived by substituting Ni for Mg was improved to three times that of cordierite. Based on the new knowledge, Ohsato et al. proposed the synthesis of indialite with superior microwave dielectric properties [17]. The indialite, being a high-temperature form, could not be synthesised by the solid-state reaction because the order-disorder phase transition is hindered by the incongruent melting to form mullite and liquid. On the other hand, indialite is an intermediate phase during the crystallisation process from glass with a cordierite composition to cordierite, as shown in **Figure 4**.

Therefore, fabrication of indialite glass ceramics has been attempted [17, 39]. Although the indialite is a metastable phase transforming to cordierite at higher temperatures, it is a relatively stable phase which occurs in nature formed by the crystallisation of natural glass. As this occurrence is in India, the mineral was named indialite. Another phase of μ-cordierite precipitating in the early stage of the crystallisation of cordierite glass is β-quartz solid solutions. The naming of μ-cordierite is not correct because of the different crystal structure, so the name that should be used is β-quartz solid solutions [38].

The cordierite composition was melted at 1550°C and was cast into a cylindrical rod with the diameter φ = 10 mm and l = 30 mm in a graphite mould. In order to avoid fracture due to internal strain, the cast glass rod was annealed at 760°C below

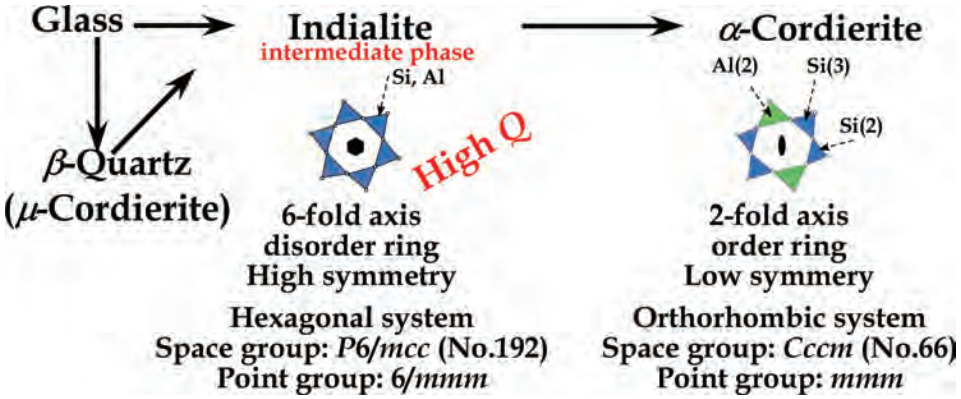

Figure 4.
Polymorphism of cordierite: indialite is the high temperature/high symmetry form, and cordierite is the low temperature/low symmetry form. In addition, indialite is an intermediate phase during crystallisation from glass to cordierite.

the glass transition point of 778°C [38]. The 10 mm diameter glass rod was cut to form a resonator with a height of 6 mm. The glass pellets were crystallised at temperatures in the range 1200–1470°C/10 and 20 h. The crystallised pellets had two problems: deformation by the formation of glass phase and cracking by anisotropic crystal growth from the surface (**Figure 5(a)**) [39]. **Figure 5(b)** and **(c)** shows photographs taken by a polarising microscope of a thin section of the crystallised samples. The needle-like crystals grown from the surface had an orientation with *c*-axis elongation. The microwave dielectric properties of the sample with cracking had a wide scattering range of the data [17, 39].

Figure 6(a) shows the volume of indialite/cordierite examined by the Rietveld method [40], which is estimated with two phases such as indialite and cordierite. Hereabout, the residual % is compared to that of cordierite. At 1200°C, the precipitated phase of indialite was about 96.7%. The volume of indialite reduced as the temperature and to 17.1% (82.9% for cordierite) at 1400°C. **Figure 6(b)** and **(c)** shows the microwave dielectric properties of indialite/cordierite glass ceramics and remarkably high *Qf* value of more than 200 × 10^3 GHz at 1300°C/20 h [17]. This is much better than the highest *Qf* value of 100 × 10^3 GHz obtained by substitution with Ni using the conventional solid-state reaction as previously described (**Figure 2(b)**) and is feasible for millimetre-wave dielectrics. The *Qf* values decreased as crystallisation temperature. In comparison with the amount of indialite as shown in **Figure 6(a)**

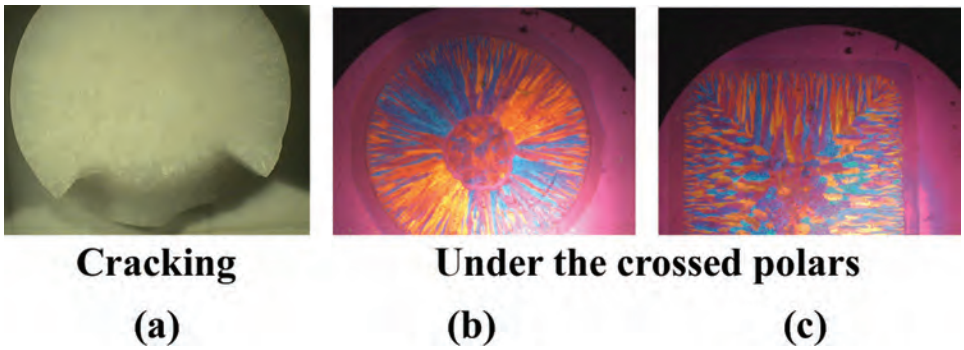

Figure 5.
Cracking of crystallised pellets (a) and anisotropic crystal growth of the pellets under the crossed polars with a sensitive test plate (b) and (c).

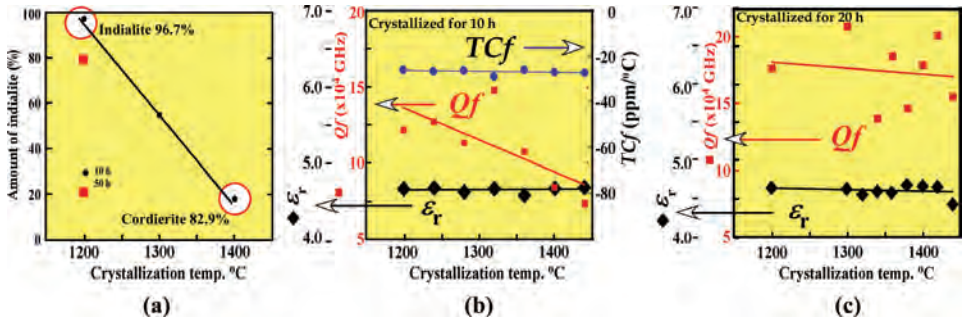

Figure 6.
Amount of indialite (a) and microwave dielectric properties of crystallised indialite at 1200–1440°C for 10 (b) and 20 (c) hours.

[39] and its *Qf* values as shown in **Figure 6(b)** and **(c)** [17], it is clear that the indialite glass ceramics present a higher *Qf* than that of cordierite. The ε_r was the lowest among the silicates, about 4.7 as shown in **Figure 6(b)** and **(c)**, and the *TCf* was −27 ppm/°C as shown in **Figure 6(b)**. Therefore, from these figures, indialite shows a higher *Qf* than cordierite. This *TCf* value of −27 ppm/°C is better than that of other silicates having a low *TCf* of approximately −60 ppm/°C [39].

2.1.3 Conclusions for indialite/cordierite glass ceramics

- Indialite/cordierite glass ceramics are one of the examples of high symmetry bringing a higher *Q* than ordering by order-disorder transition. Indialite glass ceramics with disordered high symmetry have higher *Qf* properties than cordierite with ordered low symmetry.

- Cordierite with substituted Ni for Mg synthesised by solid-state reaction exhibited an improved *Qf* from 40 × 10^3 to 100 × 10^3 GHz (**Figure 2(b)**). Rietveld crystal structure analysis showed that the cordierite was transformed to indialite [16].

- A novel idea from glass ceramics suggested the fabrication of indialite as an intermediate phase. Glass ceramics crystallised at 1200°C were almost completely indialite at 96.7% with a high *Qf* of 150 × 10^3 GHz, and those crystallised at 1400°C were cordierite at 82.9% with a lower *Qf* of 80 × 10^3 GHz. (**Figure 6**) [17, 39].

- Indialite/cordierite crystallised from cordierite glass at 1300°C/20 h showed good microwave dielectric properties of ε_r = 4.7, *Qf* > 200 × 10^3 GHz and *TCf* = −27 ppm/°C (**Figure 6**) [17, 39].

2.2 Pseudo tungsten-bronze solid solutions: compositional ordering bringing high *Q*

2.2.1 Introduction

The pseudo tungsten-bronze solid solutions $Ba_{6-3x}R_{8+2x}Ti_{18}O_{54}$ (*R* = rare earth) located on the tie-line of $BaTiO_3$-$R_2Ti_3O_9$ are shown in **Figure 7(a)** and have been utilised in mobile phones because of their high dielectric constant of 80–90 [20, 21]. This solid solution was first reported by Varfolomeev et al. [41], based on Nd and Sm systems. The composition ranges 0.0 < < *x* < < 0.7 for *R* = Nd and 0.3 < < *x* < < 0.7 for

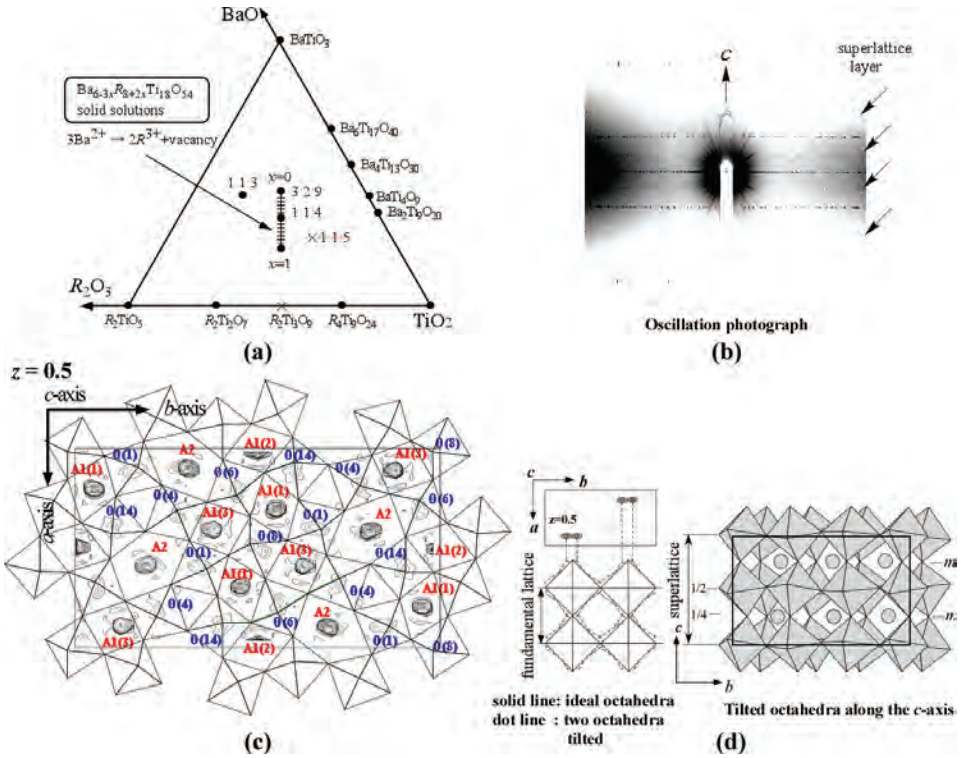

Figure 7.
A part of the BaO-R_2O_3-TiO_2 ternary phase diagram with pseudo tungsten-bronze type solid solutions (a). Oscillation photograph along c-axis of pseudo tungsten-bronze type solid solutions (b). Electron density map (Fourier map) of the fundamental structure superimposed on a superstructure framework (c) and TiO_6 tilting octahedra along the c-axis on the super-lattice (d) deduced from the splitting of oxygen in the fundamental structure (c), and the splitting of oxygen atoms based on the tilting of octahedra as shown in left side figure of the fundamental lattice (d). Right side schematic figure: super structure produced by tilting octahedral (d).

Sm [42] were reported by Ohsato et al. [19] and Negas et al. [43]. The composition range of the solid solutions becomes narrower with the decrease in the ionic radius of the *R*-ion, and Ga and Eu form only $BaO{\cdot}R_2O_3{\cdot}4TiO_2$ composition [44].

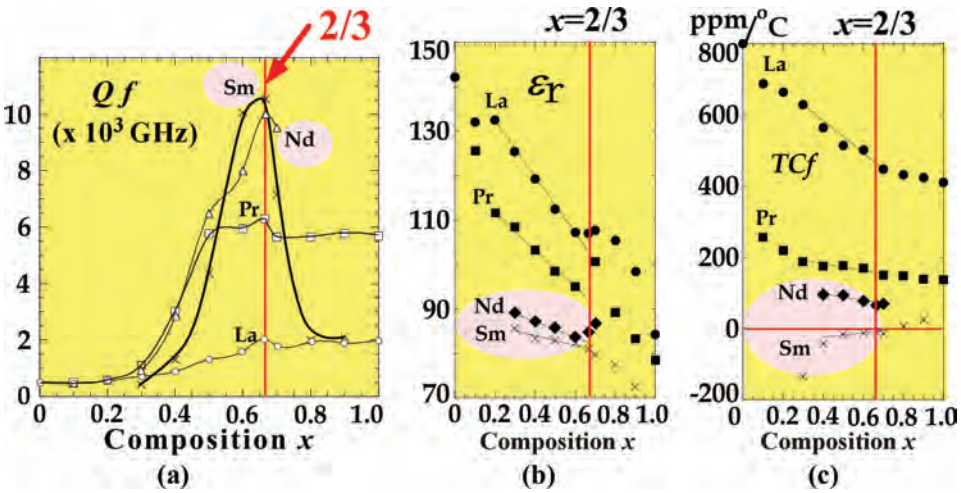

Figure 8.
Qf (a), ε_r (b) and TCf (c) of Sm, Nd, Pr and La system as a function of composition x.

Ohsato et al. and Negas et al. reported the microwave dielectric properties for the Sm, Nd, Pr and La systems as a function of composition x as shown in the **Figure 8(a)** [20, 43, 45] and Fukuda et al. reported the Pr system [46]. On the solid solutions, the composition with x = 2/3 was found by Ohsato et al. [42], at which the Qf value becomes the highest due to the ordering in the rhombic and pentagonal sites. The dielectric constants ε_r and TCf (**Figure 8(b)** and **(c)**) are decreased as a function of the composition x and are affected by volume and tilting angle of the TiO_6 octahedra and the polarizabilities of R and Ba ions [20]. The Clausius-Mosotti equation determined the temperature coefficient of the dielectric constant $TC\varepsilon_r$ as a function of the ratio of the mean radii (r_a/r_b) of A- and B-site ions by Valant et al. [47]. Hither, ra/rb is connected to the tilting of the TiO_6 octahedra. In this study, on the system without order-disorder phase transition that is without symmetry change, it is discussed that the ordering especially compositional ordering brings high Qf.

2.2.2 Crystal structure of pseudo tungsten-bronze solid solutions

2.2.2.1 Structure

The crystal structure of the pseudo tungsten-bronze $Ba_{6-3x}R_{8+2x}Ti_{18}O_{54}$ (R = rare earth) solid solutions [48–51] includes the perovskite blocks of 2 × 2 unit cells with rhombic ($A1$) sites and pentagonal ($A2$) sites, as shown in **Figure 9**, which are named after the tetragonal tungsten-bronze structure with 1 × 1 perovskite blocks and pentagonal sites [20, 48, 50]. On this compound, two large sites including Ba- and R-ions are placed such as $A1$ and $A2$. The Ba-ions engaged on the pentagonal $A2$-sites and R-ions $A1$-sites on the perovskite blocks. Two more sites, B and C are positioned on the tungsten-bronze crystal structure. The B-site is the same as the TiO_6 octahedral place in the perovskite, and the C-site is a triangular site which is usually empty. This crystal structure of this compound has a special relationship with the perovskite structure. If the two ions are the same size, the structure will change to perovskite with only an $A1$-site owing to the combination of the

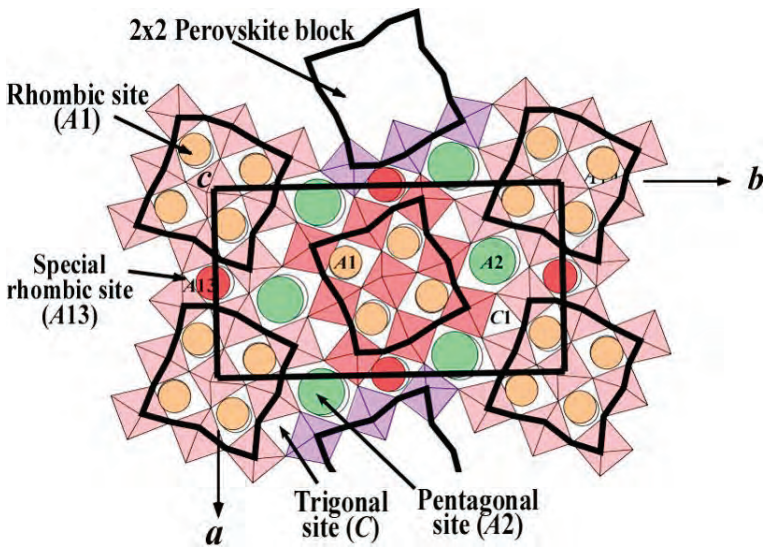

Figure 9.
Crystal structure of the pseudo tungsten-bronze solid solutions. Rhombic (A1) sites located in 2 × 2 unit cells of perovskite blocks, and pentagonal (A2) and trigonal sites (C).

pentagonal *A*2-site and the trigonal *C*-sites [20, 52]. The crystal data are as follows: orthorhombic crystal system of space group *Pbnm* (No. 62), point group *mmm* and lattice parameters a = 12.13, b = 22.27, c = 7.64 Å, Z = 2 and Dx = 5.91 g/cm^3.

2.2.2.2 Tilting

The structure has a super lattice along the *c*-axis with a double lattice of perovskite as shown in **Figure 7(b)** of an oscillation photograph with super diffraction lines [53, 54]. The crystal data of the fundamental lattice are as follows: orthorhombic crystal system of space group *Pbam* (No. 55), point group *mmm* and lattice parameters a = 12.13, b = 22.27, c = 3.82 Å, Z = 1 and Dx = 5.91 g/cm^3. The super lattice is depending on the tilting of TiO_6 octahedra as shown in **Figure 7(d)**. The tilting was endowed in the density map (**Figure 7(c)**) which is of the fundamental lattice superimposed on a superstructure framework. The top oxygen ions (O(1), O(4), O(6), O(8) and O(14)) of octahedra are separated into two along the *c*-axis. The left figure of **Figure 7(d)** shows the reason for splitting of the top oxygen [20]. However, this super lattice is not depending on the order-disorder phase transition as complex perovskite as explained at 2.3 section. The tilting of octahedra might be depending on the size of *A*-ion in the perovskite block.

2.2.2.3 Compositional ordering

The chemical formula of the solid solutions is $Ba_{6-3x}R_{8+2x}Ti_{18}O_{54}$, and the structural formula is $[Ba_4]_{A2}[Ba_{2-3x}R_{8+2x}]_{A1}Ti_{18}O_{54}$. Here, the amount of Ba in the *A*1-sites becomes zero ($2 - 3x = 0$), that is, x = 2/3. This composition is special as the following sentence: the structural formula is $[Ba_4]_{A2}[R_{8+4/3}]_{A1}Ti_{18}O_{54}$ which is occupied separately by Ba in *A*2 and by *R* in *A*1 as shown in **Figure 10(b)**. This special composition is called "compositional ordering" [20, 21, 42].

2.2.3 Microwave dielectric properties of pseudo tungsten-bronze solid solutions

Figure 8 shows the microwave dielectric properties of the solid solutions as a function of composition x of $Ba_{6-3x}R_{8+2x}Ti_{18}O_{54}$ [20, 21, 42]. The quality factor (Qf) changes nonlinearly and has the highest value at particular point x = 2/3 with compositional ordering specified above [55]. The highest Qf value might be depending on the internal strain. **Figure 11(a)** confers internal strain η obtained from the slope of equation $\beta\cos\theta = r/t + 2\eta\sin\theta$. The internal strain η of the special point x = 2/3 is the lowest with the compositional ordering as a function of composition x as shown

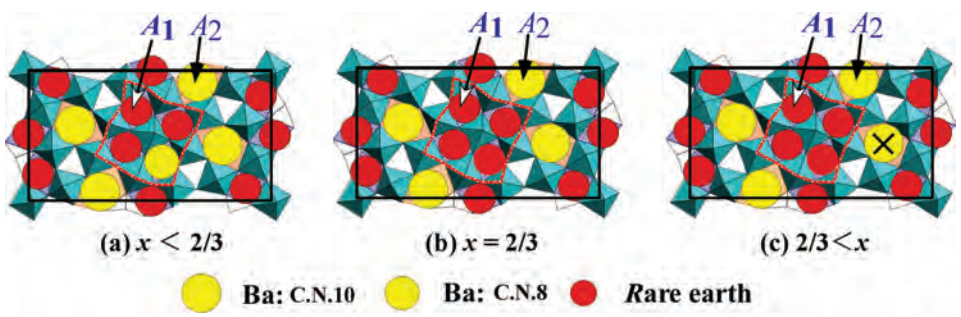

Figure 10.
Structure of disordering (a), compositional ordering (b) and defects in A2-sites (c), depending on the x values of $Ba_{6-3x}R_{8+2x}Ti_{18}O_{54}$.

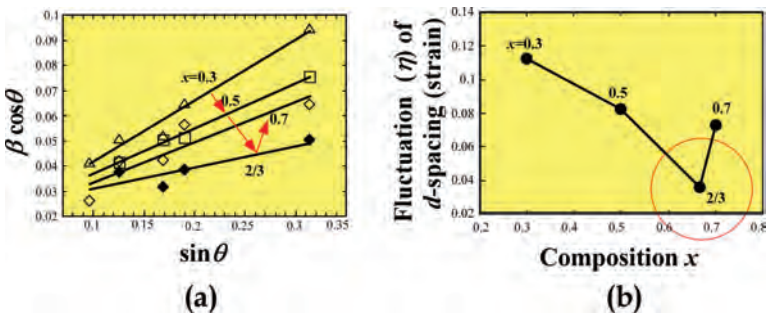

Figure 11.
Internal strain η values obtained from the slope of equation βcosθ = r/t + 2ηsinθ as a function of sinθ for x = 0.3, 0.5, 2/3 and 0.7 (a) and strain η (d-spacing) as a function of composition x (b).

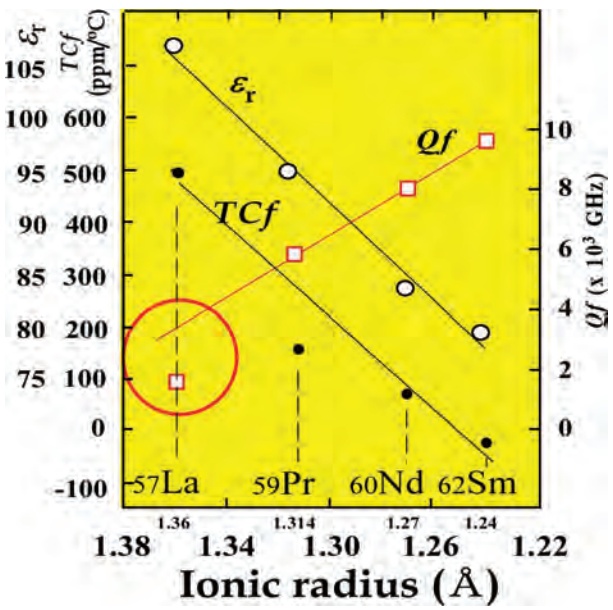

Figure 12.
Microwave dielectric properties as a function of ionic radius of R ion.

in **Figure 11(b)**. The internal strain comes from the fluctuation of *d*-spacing of the lattice broadening the full width at half maximum (FWHM) [20, 21, 56].

The *Qf* value at the special point $x = 2/3$ shows the highest of 10.5×10^3 GHz in the Sm system, 10.0×10^3 GHz in the Nd system and 2.0×10^3 GHz in the La system as depicted in **Figure 8(a)** [20, 21, 56]. The *Qf* values reducing in the order of Sm, Nd, Pr and La are depending on the ionic radius relating size difference between Ba and *R* [57], and that of La is deviating from the *Qf* line through the Sm, Nd and Pr as shown in **Figure 12**. If the sizes are similar, the crystal structure should become perovskite structure. In the case of Sm, the difference is maximum which introduces the stability of the crystal structure. The size of La ion is similar to Ba, so the structure might be unstable to be low *Qf*.

2.2.4 Symmetry and ordering for Q

On the microwave dielectrics, high *Q* has been brought by a high potential material, which has an over-well-proportional rigid crystal structure with symmetry

[11–13]. That is, the structure should be without electric defects, nondistortion and strain. Complex perovskites were described later, it is believed that ordering by long time sintering brings high *Q*, but we are pointing out symmetry is the predominant factor [14, 15]. In the case of indialite/cordierite, indialite with high symmetry shows higher *Q* than cordierite with ordering [17, 18, 39]. This case has an order-disorder phase transition. On the other hand, in the case of pseudo tungsten-bronze solid solutions which has no phase transition, one of ordering that is the compositional ordering brings high *Q* [20, 21]. In the case of no symmetry change, ordering is predominant.

2.2.5 Conclusions for pseudo tungsten-bronze

- The pseudo tungsten-bronze solid solutions have been used for mobile phones for miniaturisation based on their high *Qf* and high ε_r.
- The compound has a unique point of $x = 2/3$ on the $Ba_{6-3x}R_{8+2x}Ti_{18}O_{54}$ chemical formula which shows the highest *Qf* value.
- The special point of $x = 2/3$ on the structural formula of $[Ba_4]_{A2}[Ba_{2-3x}R_{8+2x}]_{A1}Ti_{18}O_{54}$ is the composition at which Ba-ions disappear on the *A*1-sites because $2 - 3x = 0$. That is the point of compositional ordering.
- The compositional ordering brings high *Q* by maintaining the stability of the crystal structure.

2.3 Complex perovskites

There are many kinds of complex perovskites such as 1:1, 1:2 and 1:3 type in *B*-site and 1:1 type in *A*-sites [21]. In this chapter, 1:2 type complex perovskite compounds $A^{2+}(B^{2+}_{1/3}B^{5+}_{2/3})O_3$ are presented such as $Ba(Zn_{1/3}Ta_{2/3})O_3$ (BZT), $Ba(Mg_{1/3}Ta_{2/3})O_3$ (BMT) and $Ba(Zn_{1/3}Nb_{2/3})O_3$ (BZN). These complex perovskite compounds have order-disorder phase transitions (**Figure 13(a)** and **(b)**) [58]. The ordered phase that appears at low temperatures is a trigonal (rhombohedral) structure of space group $P\bar{3}m1$ (No. 164), and the disordered phase appearing at high temperatures is a high symmetry cubic structure of $Pm\bar{3}m$ (No. 221), as shown

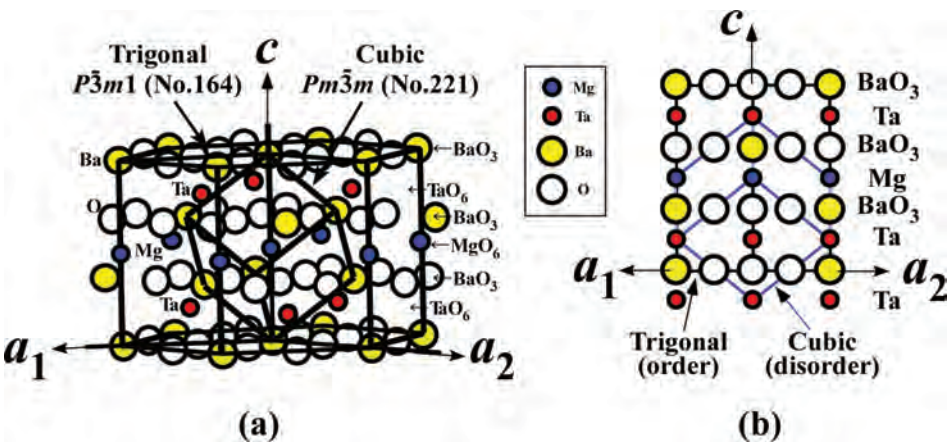

Figure 13.
Complex perovskite crystal structure composed by Mg/TaO_6 octahedra located between BaO_3 closed packing layer, showing relationship between cubic and trigonal crystal lattice. Perspective figure (a) and (110) plane (b).

in **Figure 13** [21]. In the ordered form of BMT, Mg^{2+} and Ta^{5+}-ions located among the adjacent packing layers of BaO_3 are ordering as -Mg-Ta-Ta-Mg-Ta-Ta-Mg-, as shown in **Figure 13**. On the other hand, in the disordered form, Mg^{2+} and Ta^{5+}-ions occupy *B*-sites statistically.

2.3.1 Introduction

Kawashima et al. [14] presented that ordering brings a high *Q* based on BMT with long duration sintering, which showed high *Qf* and ordering. This has previously been believed to be the case because long duration sintering samples generally show high *Qf* and ordering. However, some examples have arisen that contradict this relation, such as BMT-$Ba(Co_{1/3}Ta_{2/3})O_3$ [59], BMT-$BaZrO_3$ [60], BMT-$BaSnO_3$ [61] and BZT-$(SrBa)(Ga_{1/2}Ta_{1/2})O_3$ [62]. Koga et al. [23–26] presented the relationship between high *Qf* and the ordering ratio as determined by the Rietveld method, the high *Qf* samples with disordered structure synthesised by spark plasma sintering (SPS) [63] and the effects of annealing of disordered BZN with an order-disorder transition point of 1350°C [26]. HRTEM and Rietveld studies confirmed the ordering and disordering of BZN samples [64]. Partial ternary phase diagrams such as BaO-ZnO-Ta_2O_5, BaO-MgO-Ta_2O_5 and BaO-ZnO-Nb_2O_5 were studied on the composition with high *Qf* that deviated from the stoichiometric composition of BZT/BMT/BZN by Kugimiya et al. [22, 27], Koga et al. [24, 26] and Kolodiazhnyi [29]. Kugimiya pointed out that the solid solutions with high density and high *Qf* located on the tie-line BMT-$Ba_5Ta_4O_{15}$, which have completed the ideal chemical formula without oxygen defects. It is one of the conditions for high *Q* that the high compositional density brings high *Qf*.

2.3.2 Origin of high Q for microwave complex perovskite

In this section, it is explained that ordering has no relation with *Qf* based on the following three sets presented by Koga et al. [23, 25, 26, 63].

2.3.2.1 Ordering ratio and Qf

The ordering of BZT was observed on the samples with high *Qf* sintered at 1350°C [23] over 80 h. **Figure 14** presents the XRPD patterns (**a**) with super lattice lines (asterisked), and the high angle diffraction patterns (**b**) which depicts splitting of 420 cubic diffraction peak into two peaks, namely 226 and 422 in the trigonal system. These data are consistent with the report by Kawashima et al. [14].

Koga et al. investigated the amount of BZT ceramic as ordering ratio by the Rietveld method [23], which is shown in **Figure 15(a)**. The ordering ratio saturates at about 80%, but the *Qf* values increase up to 100×10^3 GHz. This shows that the effect of ordering on the *Qf* is not so significant. However, the *Qf* values are affected by density and grain size as shown in **Figure 15(b)** and **(c)**, respectively [15, 23].

2.3.2.2 BZN with a clear order-disorder transition

Many complex perovskites such as BMT and BZT have the order-disorder phase transition at high temperature, and the order-disorder transition is not so clear. On the other hand, BZN shows clearly the phase transition at lower temperature 1350°C [26]. **Figure 16(a)** shows *Qf* as a function of sintering temperature. Under the transition temperature such as 1200 and 1300°C, the sintered samples show order with under 50×10^3 GHz of *Qf*. Moreover, at 1400°C, higher than the transition

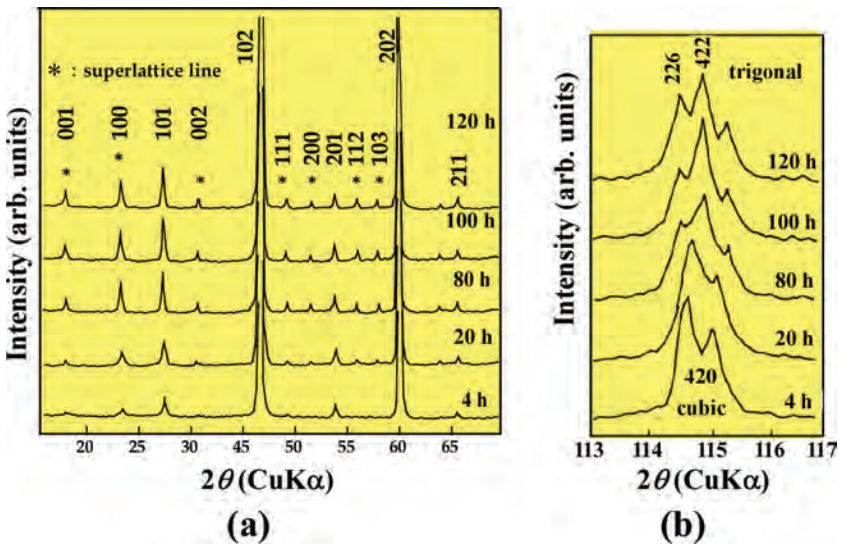

Figure 14.
XRPD patterns of BZT ceramics with different sintering times at 1350°C (a), here, asterisks are super lattice diffractions, and Magnified XRPD patterns around 2θ = 115° in which 420 diffraction peak split to 226 and 422(b).

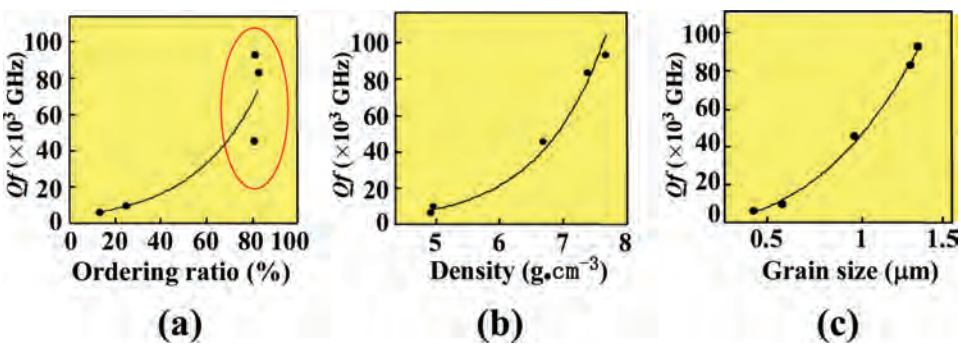

Figure 15.
The Qf as functions of ordering ratio (a), density (b) and grain size (c) of BZT ceramics.

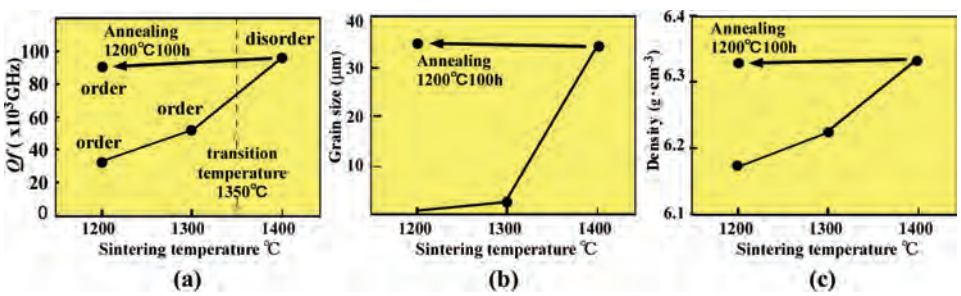

Figure 16.
Qf (a), grain size (b) and density (c) as a function of sintering temperature of BZN ceramics.

temperature, the *Qf* values increased to 90 × 10^3 GHz with disordering structure. This shows that the high symmetry form with disorder performs higher *Qf* than ordering form. Moreover, the sample annealed at 1200°C/100 h transformed to order form, but the *Qf* value did not improve and slightly decreased. Grain size and

densities as shown in **Figure 16(b)** and **(c)** also increased as the sintering temperature from 1200 to 1400°C [15, 26]. As if the sample sintered at 1400°C annealed at 1200°C/100 h, the grain size and densities were not changed. Because of annealing, the slight decrease in *Qf* might be a result of the low symmetry that accompanies order. On the contrary, Wu et al. [65] presented annealing of BZN at 1300°C brings high *Qf* with ordering. The annealing temperature is high enough for sintering, so sintering was proceeded with ordering the same as Kawashima's results [14].

The BZN samples A and B are also studied by XRPD and HRTEM, which sintered at 1400°C/100 h above the order-disorder phase transition point and subsequently annealed at 1200°C/100 h below the transition point, respectively [26, 64]. The two samples were identified by conventional XRPD as shown in **Figure 17(a)**. As the super lattice lines are not clear, the high angle XRPD patterns around 2θ~115° were measured (**Figure 17(b)**). On the XRPD pattern, the sample A shows a single peak of the 420 diffraction, so it was confirmed as disorder phase. On the other hand, the sample B shows the peak splitting of 422 and 226 depending ordering. These results are comparable with Koga's data [23]. These two samples were analysed by the Rietveld method.

HRTEM figures as shown in **Figure 18** for most area of sample A (**Figure 18(a)**) and B (**Figure 18(c)**) are disordered and ordered area along the [111]c direction, respectively. A fast Fourier transform (FFT) image is inserted in **Figure 18(a)** of a disordered area without further reflections along the [111]c direction and in **Figure 18(c)** of a ordered area with additional two reflection points for super lattice. In the both sample A and B, mixed area of disordered and ordered area existed in **Figure 18(b)**, and in the sample B, ordered area showing twin-related anti-phase domain boundary also existed as shown in **Figure 18(d)**. The FFT image of twin area shows superimposed of ordered diffractions with four additional points.

Figure 19 depicts the high-resolution XRPD pattern of sample A and B using synchrotron radiation [64]. The super lattice diffraction 100 t peaks (reciprocal lattice plane 100 in the trigonal crystal system) are observed in both samples. The diffraction intensity of sample A is lower than that of sample B. These super lattice diffraction intensity peaks are comparable with the ordering ratios, that is the sample A and B have the value of 27.6 and 54.2%, respectively, obtained by the Rietveld method. Although the degree of ordering of sample B is large compared to that of sample A, it was assumed about 80% ordering for a whole sample, as in the case of BZT [23].

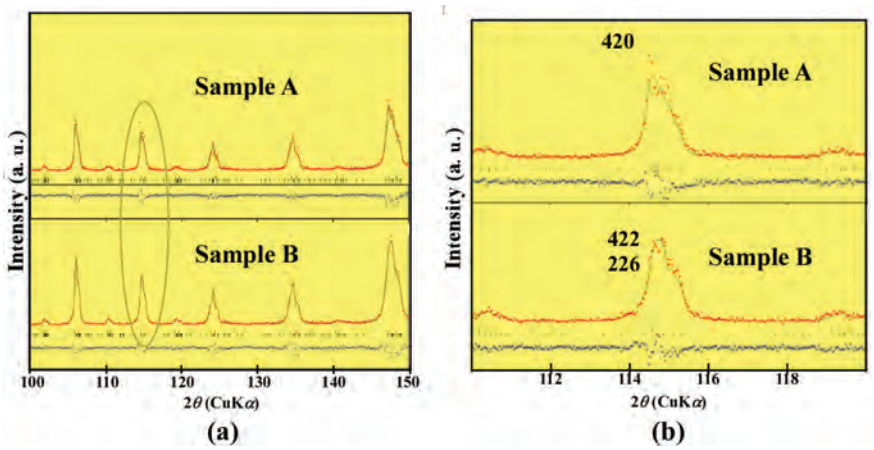

Figure 17.
XRPD patterns for BZN ceramics sintered at 1400°C (sample A) and annealed at 1200°C (sample B) (a) and magnified high angle XRPD patterns around 2θ~115° (b).

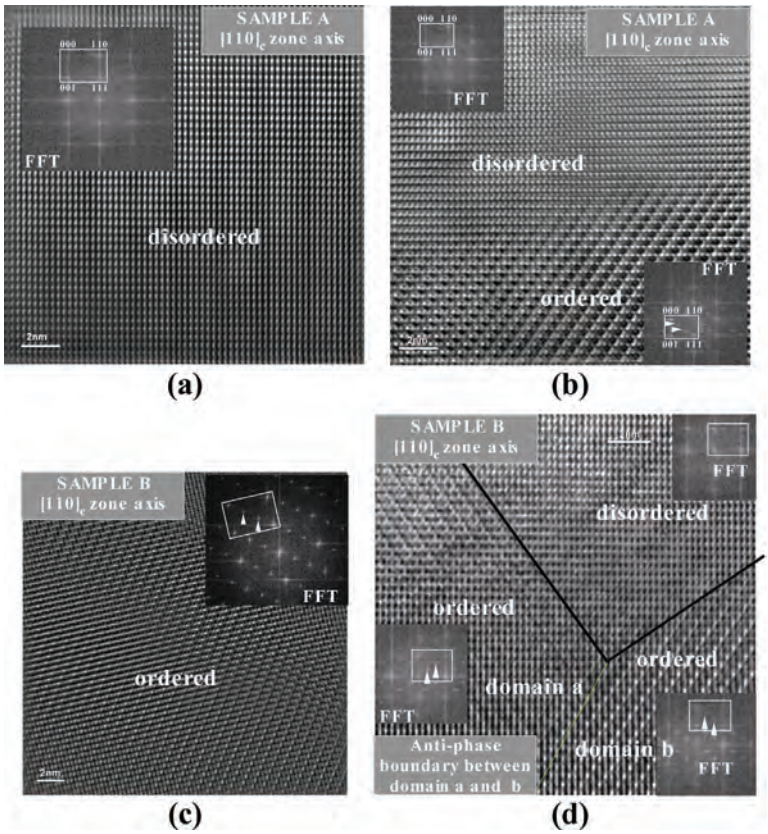

Figure 18.
HRTEM images of sample A and B with FFT image along the [111]c direction: disordered area in sample A (a), mixed area of disordered and ordered area in sample A (b), ordered area in sample B (c) and twin related anti-phase domain boundary in sample B (d).

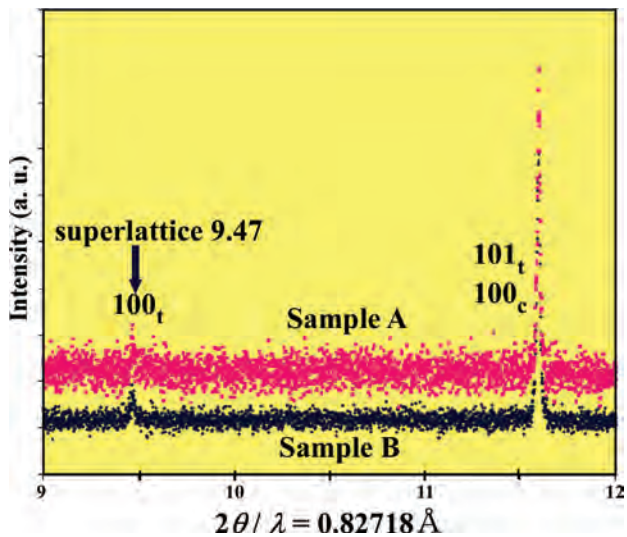

Figure 19.
High-resolution synchrotron XRPD patterns (λ = 0.82718 Å) for sample A and B with super lattice peak 100_t. Here, subscript t is trigonal, and c is cubic.

It is revealed that the degree of ordering increased from 27.6 to 54.2% due to the annealing. However, the *Qf* values, grain size and the density have no influence on the degree of ordering (**Figure 16**). While the disordered area of sample A (sintered above the transitional temperature) changes to the low-temperature phase with ordering by the annealing, the *Qf* values were expected to be increased. However, the *Qf* values changed only somewhat from 95.7 × 10^3 GHz to 95.0 × 10^3 GHz [64]. The effect of ordering is not acceptable to change the *Qf* value considerably.

2.3.2.3 BZT with disordering leaded high Qf by SPS

The ordered and disordered BZT ceramics can be achieved by varying the sintering duration in the conventional solid-state reaction (SSR). A high density and high *Q* ceramics of ordered BZT were obtained by SSR with a long sintering time of over 80 h, while the disordered BZT was not possible to fabricate by using SSR. Koga et al. [63] reported the high density disordered BZT ceramics for a short sintering time of 5 mins by using spark plasma sintering (SPS). **Figure 20(a)** presents the *Qf* as a function of the densities of BZT fabricated using SSR and SPS [15, 63]. The fabricated SPS samples were shown to be disordered cubic type of perovskite as depicted in the XRPD pattern (**Figure 20(b)**) with a peak of 420 reflection in compared with the ordered trigonal type with peaks separations of 422 and 226 when sintered using SSR (1400°C 100 h). The ceramics were sintered at the temperature between 1150 and 1300°C under 30 Mpa pressure [63].

This may result in the disordered BZT with a high density of 7.62 g/cm^3, which is approximately 20% higher than that of low-density samples of 5.0–6.0 g/cm^3 synthesized by conventional SSR. The full width at half maximum (FWHM) of the 420 peak became narrower with an increase in the temperature from 1100 to 1300°C (**Figure 20(b)**) indicates that the degree of crystallisation of the disordered cubic phase is improved without the need for conversion to the ordered trigonal phase. Regardless of the method of synthesis, *Qf* is strongly dependent on density, and *Qf* values were improved with increasing density. The dense disordered BZT ceramics synthesized by SPS showed a significantly high *Qf* (= 53.4 × 10^3 GHz) comparable to that of the ordered BZT with the same density (= ca. 7.5 g/cm^3) synthesized by SSR. The crystallisation with densification of BZT ceramics should play a more critical role in the improvement of the *Q* factor in the BZT system rather than the structural ordering.

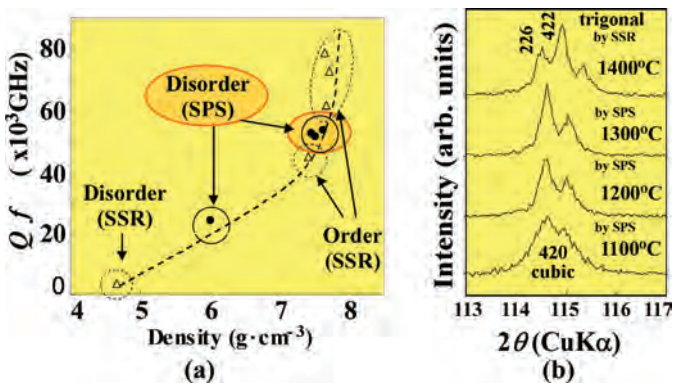

Figure 20.
Qf of BZT by solid-state reaction (SSR) and spark plasma sintering (SPS) as a function of density, Disordered BZT by SPS shows high Qf (a). Nonsplitting XRPD patterns around 420 diffraction of BZT sintering by SPS with different sintering temperatures compared with ordered sample by SSR with splitting pattern (b).

2.3.3 Deviated compositions with high Qf from stoichiometric complex perovskite composition

In a BaO-Mg/ZnO-Ta_2O_5 partial ternary ceramic (BMT/BZT system), complex perovskite such as BMT and BZT are forming solid solutions, and the *Qf* values varied intrinsically based on the crystal structure in the solid solutions depending on the density and defects. In this section, the crystal structure and properties on the varied compositions from the stoichiometric complex perovskite composition are reviewed for high *Qf* research.

2.3.3.1 The highest Qf composition with intrinsic compositional density by Kugimiya's research

Kugimiya [22, 27] presented the highest *Qf* composition with intrinsic compositional density on the Ta and Ba rich side near the BMT-$Ba_5Ta_4O_{15}$ tie-line in a BaO-MgO-$TaO_{5/2}$ partial system (BMT system), as shown in **Figure 21**. He presented three areas divided by the following two lines as shown in **Table 1** and **Figure 21**.

$$\alpha = 5\gamma/4 \tag{3}$$

$$\alpha = \gamma/2 \tag{4}$$

Here, α and γ are as written in the formula $\alpha BaO{\cdot}\gamma TaO_{5/2}$. On the $\alpha = 5\gamma/4$ line, $Ba_{1+\alpha}(Mg_{1/3}Ta_{2/3} + {}_{4\alpha/5}V_{\alpha/5})O_{3+3\alpha}$ solid solutions are formed as the ideal compositions without vacancies in the *A*- and O-sites. In the *B*-site, the vacancy is neutralized and without charge.

In **Figure 21**, the composition with intrinsic compositional high density shows the highest *Q* of 50.0×10^3 on the tie-line between BMT and $Ba_5Ta_4O_{15}$ ($\alpha = 5\gamma/4$). The contour lines in **Figure 21** show *Q* values from 2.0×10^3 in the outer area to 25.0×10^3 in the centre. The contour is elongated parallel to the *Q* max line as drawn in **Figure 21,** and it changes steeply on the perpendicular to this line. So, the compositions without oxygen vacancy and with neutralised charge vacancies

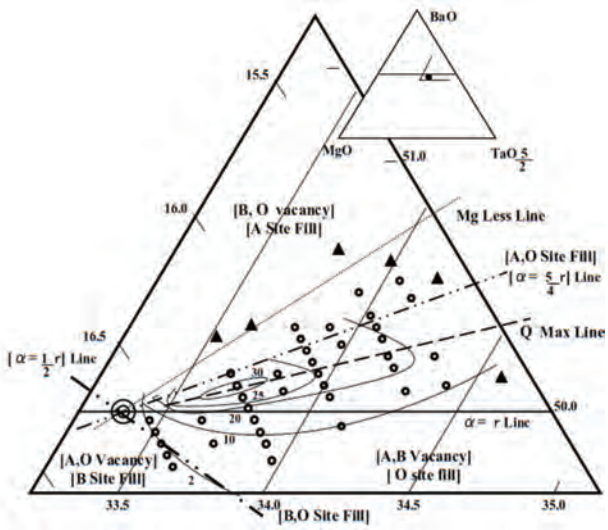

Figure 21.
BaO-MgO-$TaO_{5/2}$ partial system (BMT system).

α	Chemical formula	Vacancy
$\alpha > 5\gamma/4$	$Ba_{1+\alpha}(Mg_{1/3}Ta_{2/3+}\gamma V_{\alpha-\gamma})O_{3+\alpha+5\gamma/2}\,V_{2\alpha-5\gamma/2}$	*A*: fill, *B*, O: vacancy
$\alpha = 5\gamma/4$	$Ba_{1+\alpha}(Mg_{1/3}Ta_{2/3+4\alpha/5}V_{\alpha/5})O_{3+3\alpha}$	*A*, O: fill, *B*: vacancy
$5\gamma/4 > \alpha > \gamma/2$	$Ba_{1+\alpha}V_{5\gamma/6-2\alpha/3}(Mg_{1/3}Ta_{2/3+\gamma}\,V_{\alpha/3-\gamma/6})\,O_{3+\alpha+5\gamma/2}$	*A*, *B*: vacancy, O: fill
$\alpha = \gamma/2$	$Ba_{1+\alpha}V_{\alpha}(Mg_{1/3}Ta_{2/3+\gamma})O_{3+6\alpha}$	*A*: vacancy, *B*, O: fill
$\alpha < \gamma/2$	$Ba_{1+\alpha}V_{\gamma-\alpha}(Mg_{1/3}Ta_{2/3+\gamma})O_{3+\alpha+5\gamma/2}\,V_{\gamma/2-\alpha}$	*A*, O: vacancy, *B*: fill

Table 1.
*The chemical formula for three areas divided by two lines: $\alpha = 5\gamma/4$ and $\alpha = \gamma/2$, here, α and γ are in $Ba_{\alpha}Ta_{\gamma}O_{\alpha+5\gamma/2}$ and vacancies on the **A**-, **B**- and O-sites [22].*

are ideal for microwave dielectrics, and the density is high due to the partial substitution of Ta in the site of Mg, which is denoted as intrinsic compositional density [28]. Other regions have some defects degrading the *Qf* values, which were explained on the references [21, 22, 27, 28].

2.3.3.2 Phase conditions in the vicinity of BZT by Koga's research

Koga et al. [24, 25] showed the highest *Qf* composition shifted from the stoichiometric BZT composition. The ordering ratio of the deviated composition was not higher than that of the stoichiometric composition, which was calculated by the Rietveld method. These results were presented by the study of the phase relations in the vicinity of BZT in the BaO-ZnO-Ta_2O_5 ternary system, as shown in **Figure 22** [24, 25]. These samples were sintered at 1400°C/100 h as reported in Koga's paper. These diffraction patterns fit the Rietveld method well [23, 24]. Ordering ratios obtained are shown in **Figure 23(a)**. Three areas in the vicinity of BZT are presented as shown in **Figure 22**. 1st one (I) is ordering area with BZT single phase, the 2nd one (II) is ordering area with secondary phase and 3rd one (III) is disordering area with BZT single phase.

The first area (I) is characterised as a BZT single phase with an ordered structure and a high *Qf*. The varied compositions E and K have high *Qf* values about 50% higher than that of the stoichiometric BZT composition A. The ordering ratios at E and K are lower than that of stoichiometric BZT at A, but the density at E is the same as that of A [25]. The second (II) is composed by an ordered BZT

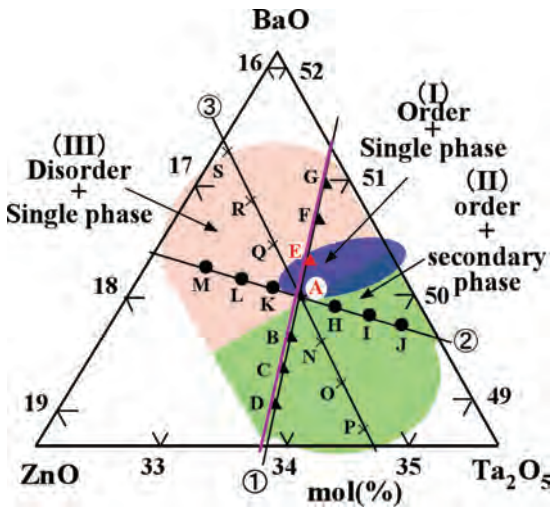

Figure 22.
Phase relations in the vicinity of BZT in the BaO-ZnO-Ta_2O_5 ternary system.

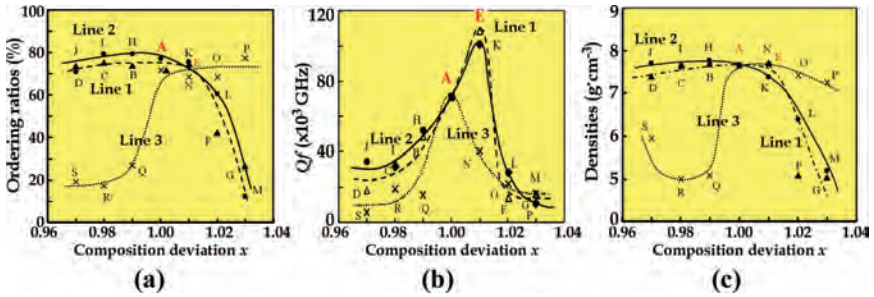

Figure 23.
Ordering ratio (a), Qf (b) and density (c) as a function of composition deviation from stoichiometric BZT.

accompanied by a secondary phase $BaTa_2O_6$ with a specific amount of Zn determined by X-ray microanalyser (XMA). The ordering ratio in this area is high at about 70–80% (**Figure 23(a)**). Although the structure is ordered, the *Qf* values decrease in the order of A-N-O-P from stoichiometric BZT (**Figure 23(b)**). The ordered BZT with the secondary phase is located on the Ta_2O_5 rich side as a eutectic phase diagram system. The third (III) with a disordered single phase shows low *Qf* and low density (**Figure 23(c)**). The low density comes from the numerous pores.

2.3.3.3 Phase conditions in the vicinity of BZT by Kolodiazhnyi's research

Kolodiazhnyi [29] also found the highest *Qf* of 330 × 10^3–340 × 10^3 GHz positions deviated from the stoichiometric BMT composition which is located in the BMT-$Ba_5Ta_4O_{15}$-$Ba_3Ta_2O_8$ compositional triangle (CT) as shown in **Figure 24**. The positions located in the single-phase BMT, which was indicated by green line. The position is close to the BMT-$Ba_5Ta_4O_{15}$ tie-line. A to H eight CTs are formed by BMT and five stable compounds, such as $Ba_5Ta_4O_{15}$, MgO, BaO, $Ba_9MgTa_{14}O_{45}$ and $Mg_4Ta_2O_9$, and three metastable compounds, $Ba_6Ta_2O_{11}$, $Ba_4Ta_2O_9$ and $Ba_3Ta_2O_8$. In A, B and C-CTs, although the samples demonstrated high density and a high degree

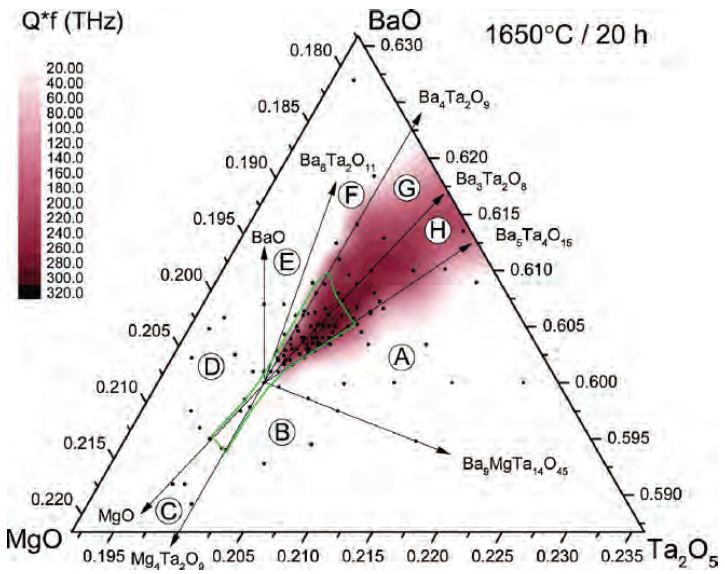

Figure 24.
Part of the BaO-MgO-Ta_2O_5 phase diagram in the vicinity of BMT divided into eight CTs. Small black dots indicate the target samples. Green line indicates an approximate boundary of the single-phase BMT.

of order, they showed low *Qf* values, attributed to the possible presence of the $Ba_9MgTa_{14}O_{45}$ second phase. Moreover, in D, E and F-CTs, as the samples were very low density, no electromagnetic resonance peaks were detected.

2.3.3.4 Koga's and Kolodiazhnyi's data comprehended in Kugimiya's data

Koga's data [24] and Kolodiazhnyi's [29] data are comparable with Kugimiya's BMT data [22]. The area (I) and the H-CT with the highest *Qf* as shown in **Figures 22** and **24**, respectively, are located on the opposite side of Kugimiya's data against the BMT-$Ba_5Ta_4O_{15}$ tie-line (**Figure 21**). These compositions will be comparable with that of the ideal crystal structure $Ba_{1+\alpha}(Mg_{1/3}Ta_{2/3+4\alpha/5}V_{\alpha/5})O_{3+3\alpha}$, as stated before in section (2.3.3.1) [22]. The formula is rewritten as $Ba(Mg_{1/3-\alpha/3}Ta_{2/3+2\alpha/15}V_{\alpha/5})O_3$ solid solutions on the tie-line BMT-$Ba_5Ta_4O_{15}$. The crystal structure in the composition region is ideal, without defects, and with an intrinsic high compositional density as described above. Surendran et al. [66] also reported a composition with high *Qf* deviated from stoichiometric BMT reviewed in detail in Intech Open Access Book [21].

2.3.4 Conclusions: important points concerning complex perovskites

- Ordering brings high *Qf* in the complex perovskite because of the long duration sintering. This situation has been bereaved for a long time. However, many examples contradicting this relation were presented.

- Koga et al. presented that *Qf* values of BZT did not depend on the ordering, preferably depending on the density and grain size.

- BZN with an order-disorder transition point at 1350°C (sample A) showed high *Qf* in the high-temperature disordered form. Moreover, annealing of the disordered sample B brings the ordered form, but the *Qf* does not improve. The both samples are analysed by the Rietveld method and HRTEM. The HRTEM presented the order form, disorder form and anti-phase domain by the FFT.

- Disordered samples with high density could not be synthesised by the solid-state reaction, but could be by SPS. The samples with disordered structure showed high *Q*. The ordering phenomenon is the only barometer of sintering in the solid-state reaction.

- Compositions deviated from stoichiometric complex perovskites such as BZT and BMT showed higher *Qf* and lower ordering than the stoichiometric composition. Based on these points, the ordering is not the reason for high *Qf*, and it is the only barometer of sintering.

- Intrinsic compositional density brings high *Qf*. On the BMT-$Ba_5Ta_4O_{15}$ tie-line, solid solutions are formed by the substitution Ta for Mg, which include high *Qf* compositions. The chemical composition with the highest *Qf* is $Ba_{1+\alpha}(Mg_{1/3}Ta_{2/3+4\alpha/5}V_{\alpha/5})O_{3+3\alpha}$, which is an ideal solid solutions without oxygen defects and neutralised vacancies (**Table 1**).

- Compositions deviated from stoichiometric BMT/BZT towards BaO and the Ta_2O_5 rich areas showing high *Qf*, as presented by Koga et al. [24], Kolodiazhny [29] and Surendran et al. [64], are comparable with intrinsic compositional density with high *Qf* as presented by Kugimiya [22].

3. Conclusions

The microwave dielectrics are the perfect, ideal and well-proportional crystal structures for low dielectric losses. Most of them belong to paraelectrics with inversion symmetry *i* and showing high symmetry and nondefects. In this chapter, the effects of ordering and symmetry were presented as follows: there are two types of ordering conditions. One is a case of nonphase transition such as pseudo tungsten-bronze solid solutions. These compounds show compositional ordering at a unique point of $x = 2/3$ on the $Ba_{6-3x}R_{8+2x}Ti_{18}O_{54}$ system, which shows the highest *Qf* without degradation of crystal symmetry. The other is a case of order-disorder phase transition such as indialite/cordierite. Indialite with a disordered structure and a high symmetry of 6/*mmm* point group has a higher *Qf* than cordierite with an ordered structure and low symmetry of *mmm* point group. It is clarified that the effect of high symmetry is predominant for high *Qf*. In the case of complex perovskite, a long sintering time of more than 80 h brings a high *Qf* accompanying ordering. It was clarified that the ordering is not necessary for high *Qf* and only a barometer of sintering in the solid-state reaction. Moreover, compositions deviated from stoichiometric complex perovskite showed higher *Qf* than the stoichiometric composition which has substituted Ta-ions for Mg/Zn-ions. The substitution brings a high density that is the compositional density. It was clarified that high compositional density brings high *Qf*.

Acknowledgements

The authors are grateful to Professors and graduate students of NIT, Meijo University and Hoseo University, and Doctors and researchers in the many companies, which collaborated with NIT. Visiting Professor Hitoshi Ohsato is grateful to the following projects: (1) support industries of Japan by Ministry of Economy, Trade and Industry (METI), Japan, (2) JSPS KAKENHI Grant Number 22560673, 25420721, JP16K06735 and (3) Nokia Foundation 2016 for Nokia Visiting Professors Project 201700003. Professor Heli Jantunen and Dr. Jobin Varghese are grateful to European Research Council Project No. 24001893 for financial assistance. The authors would also like to thank Honorary Research Professor Arthur E Hill of Salford University for valuable discussion and improving English during the preparation of this manuscript.

Author details

Hitoshi Ohsato[1,2*], Jobin Varghese[1] and Heli Jantunen[1]

1 Microelectronics Research Unit, Faculty of Information Technology and Electrical Engineering, University of Oulu, Oulu, Finland

2 Department of Research, Nagoya Industrial Science Research Institute, Nagoya, Japan

*Address all correspondence to: ohsato.hitoshi@gmail.com

References

[1] Sebastian MT. Dielectric Materials for Wireless Communication. Amsterdam: Elsevier; 2008. ISBN 13:978-0-08-045330-9

[2] Sebastian MT, Ubic R, Jantunen H. Low-loss dielectric ceramic materials and their properties. International Materials Review. 2015;**60**:392-412

[3] Ohsato H. High frequency dielectric ceramics. In: Adachi G, editor. Materials Technology Hand Book for Rare-Earth Elements. Tokyo: NTS Inc; 2008. pp. 346-358 (Japanese)

[4] Ohsato H, Kagomiya I, Chae KW. Microwave dielectric ceramics with rare-earth elements (I). Journal of the Korean Physical Society. 2012;**61**:971-979

[5] Ohsato H, Kagomiya I, Kim JS. Microwave dielectric ceramics with rare-earth (II). Integrated Ferroelectrics. 2010;**115**:95-109

[6] Ohsato H. High frequency dielectrics. In: Shiosaki T, editor. Development and Applications of Ferroelectric Materials. Tokyo: CMC; 2001. pp. 135-147 (Japanese)

[7] Wakino K. Recent development of dielectric resonator materials and filters in Japan. Ferroelectrics. 1989;**91**:69-86

[8] Tamura H. Progress of ceramic dielectric materials for microwave and millimeterwave applications. In: MWE '99 Microwave Workshop Digest. 1999. pp. 175-180

[9] Kobayashi Y, Katoh M. Microwave measurement of dielectric properties of low-loss materials by the dielectric resonator rod method. IEEE Transaction on Microwave Theory and Technologies. 1985;**33**:586-592

[10] Ichinose N. High-frequency materials and their applications. New Ceramics & Electronic Ceramics. 1996;**9**(9):1-50

[11] Ohsato H. Microwave dielectrics. In: Fukunaga O, Haneda H, Makishima A, editors. Handbook of Multifunctional Ceramics. Tokyo: NTS; 2011. pp. 152-166 (Japanese)

[12] Ohsato H. Functional advances of microwave dielectrics for next generation. Ceramics International. 2012;**38**:S141-S146

[13] Ohsato H. Design of microwave dielectrics based on crystallography. In: Akedo J, Chen XM, Tseng T, editors. Advances in Multifunctional Materials and Systems II, Ceramic Transactions. Vol. 245. Hoboken, New Jersey: Wiley; 2014. pp. 87-100

[14] Kawashima S, Nishida M, Ueda I, Ouchi H. $Ba(Zn_{1/3}Ta_{2/3})O_3$ ceramics with low dielectric loss at microwave frequencies. Journal of the American Ceramic Society. 1983;**66**:421-423

[15] Ohsato H, Koga E, Kagomiya I, Kakimoto K. Origin of high *Q* for microwave complex perovskite. Key Engineering Materials. 2010;**421-422**:77-80

[16] Terada M, Kawamura K, Kagomiya I, Kakimoto K, Ohsato H. Effect of Ni substitution on the microwave dielectric properties of cordierite. Journal of the European Ceramic Society. 2007;**27**:3045-3148

[17] Ohsato H, Kim JS, Kim AY, Cheon CI, Chae KW. Millimeter-wave dielectric properties of cordierite/indialite glass ceramics. Japanese Journal of Applied Physics. 2011;**50**(9):09NF01-1-5

[18] Ohsato H. Millimeter-wave materials. In: Sebastian MT, Ubic R,

Jantunen H, editors. Microwave Materials and Applications. Wiley; 2017. pp. 203-265

[19] Ohsato H, Ohhashi T, Nishigaki S, Okuda T, Sumiya K, Suzuki S. Formation of solid solution of new tungsten bronze-type microwave dielectric compounds $Ba_{6-3x}R_{8+2x}Ti_{18}O_{54}$ (R = Nd and Sm, $0 \leq x \leq 1$). Japanese Journal of Applied Physics. 1993;**32**:4323-4326

[20] Ohsato H. Science of tungstenbronze-type like $Ba_{6-3x}R_{8+2x}Ti_{18}O_{54}$ (R = rare earth) microwave dielectric solid solutions. Journal of the European Ceramic Society. 2001;**21**:2703-2711

[21] Ohsato H. Microwave dielectrics with perovskite-type structure. In: Pan L, Zhu G, editors. Perovskite Materials—Synthesis, Characterization, Properties, and Applications. Rijeka, Croatia: INTECH; 2016. pp. 281-330. ISBN 978-953-51-4587-5. Available from: http://cdn.intechopen.com/pdfs-wm/49723.pdf [Accessed: 15-10-2018]

[22] Kugimiya K. Crystallographic study on the Q of $Ba(Mg_{1/3}Ta_{2/3})O_3$ dielectrics. In: Abstract for Kansai branch academic meeting. 5 September 2003; Senri-life science. B-20. In: Abstract for the 10th Meeting of Microwave/Millimeterwave Dielectrics and Related Materials on the Ceramic Soc. Japan: Nagoya Institute of Technology; 21st June 2004 (Japanese)

[23] Koga E, Moriwake H. Effects of superlattice ordering and ceramic microstructure on the microwave Q factor of complex Perovskite-type oxide $Ba(Zn_{1/3}Ta_{2/3})O_3$. Journal of the Ceramic Society of Japan. 2003;**111**:767-775 (Japanese)

[24] Koga E, Moriwake H, Kakimoto K, Ohsato H. Influence of composition deviation from stoichiometric $Ba(Zn_{1/3}Ta_{2/3})O_3$ on superlattice ordering and microwave quality factor Q. Journal of the Ceramic Society of Japan. 2005;**113**:172-178 (Japanese)

[25] Koga E, Yamagishi Y, Moriwake H, Kakimoto K, Ohsato H. Large Q factor variation within dense, highly ordered $Ba(Zn_{1/3}Ta_{2/3})O_3$ system. Journal of the European Ceramic Society. 2006;**26**:1961-1964

[26] Koga E, Yamagishi Y, Moriwake H, Kakimoto K, Ohsato H. Order-disorder transition and its effect on microwave quality factor Q in $Ba(Zn_{1/3}Nb_{2/3})O_3$ system. Journal of Electroceramics. 2006;**17**:375-379

[27] Fujimura T, Nishida M, Kugimiya K. Dielectric ceramics, United patent 5,246,898

[28] Ohsato H, Koga E, Kagomiya I, Kakimoto K. Dense composition with high-Q on the complex perovskite compounds. Ferroelectrics. 2009;**387**:28-35

[29] Kolodiazhnyi T. Origin of extrinsic dielectric loss in 1:2 ordered, single-phase $BaMg_{1/3}Ta_{2/3}O_3$. Journal of the European Ceramic Society. 2014;**34**:1741-1753

[30] Miyashiro A. Cordierite–indialite relations. American Journal of Science. 1957;**255**:43-62

[31] Gibbs GV. Polymorphism of cordierite. I. Crystal structure of low cordierite. American Mineralogist. 1966;**51**:1068-1087

[32] Wu JM, Huang HL. Effect of crystallization on microwave dielectric properties of stoichiometric cordierite glasses containing B_2O_3 and P_2O_5 glasses. Journal of Materials Research. 2000;**15**:222-227

[33] Izumi F, Ikeda T. A rietveld-analysis program RIETAN-98 and its applications to zeolites. Materials Science Forum. 2000;**321-324**:198-203

[34] Toraya H, Hibino H, Ohsumi K. A new powder diffractometer for synchrotron radiation with multiple-detector system. Journal of Synchrotron Radiation. 1996;**3**:75-83

[35] Ohsato H, Kagomiya I, Terada M, Kakimoto K. Origin of improvement of *Q* based on high symmetry accompanying Si–Al disordering in cordierite millimeter-wave ceramics. Journal of the European Ceramic Society. 2010;**30**:315-318

[36] Brown ID, Shannon RD. Empirical bond-strength–bond-length curves for oxides. Acta Cryst. 1973;**A29**:266-282

[37] Brown ID, Wu KK. Empirical parameters for calculating cation–oxygen bond valences. Acta Cryst. 1976;**B32**:1957-1959

[38] Ohsato H, Kim JS, Cheon CI, Kagomiya I. Crystallization of indialite/cordierite glass ceramics for millimeter-wave dielectrics. Ceramics International. 2015;**41**:S588-S595

[39] Ohsato H, Kim JS, Cheon CI, Kagomiya I. Millimeter-wave dielectrics of indialite/cordierite glass ceramics: Estimating Si/Al ordering by volume and covalency of Si/Al octahedron. Journal of the Ceramic Society of Japan. 2013;**121**:649-654

[40] Carvajal RJ. Fullprof Software. 2006. Available from: http://www-llb.cea.fr/fullweb/powder.htm [Accessed: 13-04-2018]

[41] Varfolomeev MB, Mironov AS, Kostomarov VS, Golubtsova LA, Zolotova TA. The synthesis and homogeneity ranges of the phases $Ba_{6-x}R_{8+2x/3}Ti_{18}O_{54}$. Russian Journal of Inorganic Chemistry. 1988;**33**:607-608

[42] Ohsato H, Mizuta M, Ikoma T, Onogi Z, Nishigaki S, Okuda T. Microwave dielectric properties of tungsten bronzetype $Ba_{6-3x}R_{8+2x}Ti_{18}O_{54}$ (R = La, Pr, Nd and Sm) solid solutions. Journal of the Ceramic Society of Japan International Edition. 1998;**106-185**:184-188

[43] Negas T, Davies PK. Influence of chemistry and processing on the electrical properties of $Ba_{6-3x}Ln_{8+2x}Ti_{18}O_{54}$ solid solutions. In: Material and Processes for Wireless Communications, Ceramic Transactions 53. Hoboken, New Jersey: Wiley; 1995. pp. 196-197

[44] Valant M, Suvorov D, Kolar D. X-ray investigations and dielectric property determination of the $Ba_{4.5}Gd_9Ti_{18}O_{54}$ compound. Japanese Journal of Applied Physics. 1996;**35**:144-150

[45] Ohsato H, Ohhashi T, Kato H, Nishigaki S, Okuda T. Microwave dielectric properties and structure of the $Ba_{6-3x}Sm_{8+2x}Ti_{18}O_{54}$ solid solutions. Japanese Journal of Applied Physics. 1995;**34**:187-191

[46] Fukuda K, Kitoh R, Awai I. Microwave characteristics of mixed phases of $BaPr_2Ti_4O_{12}$-$BaPr_2Ti_5O_{14}$ ceramics. Journal of Materials Research. 1995;**10**:312-319

[47] Valant M, Suvorov D, Rawn CJ. Intrinsic reasons for variations in dielectric properties of $Ba_{6-3x}R_{8+2x}Ti_{18}O_{54}$ (R = La-Gd) solid solutions. Japanese Journal of Applied Physics. 1999;**38**:2820-2826

[48] Matveeva RG, Varforomeev MB, ll'yuschenko LS. Refinement of the composition and crystal structure of $Ba_{3.75}Pr_{9.5}Ti_{18}O_{54}$. Zhurnal Neorganicheskoi Khimii. 1984;**29**:31-34 (Trans. Russ: Journal of Inorganic Chemistry. 1984;**29**:17-19)

[49] Roth RS, Beach F, Antoro A, Davis K, Soubeyroux JL. Structural of the nonstoichiometric solid solutions $Ba_2RE_4[Ba_x+RE_{2/3-2/3x}]Ti_9O_{27}$ (RE = Nd, Sm). In: 14 Int Congress Crystallog: Mat

Sci. C-138: Collected Abstract 07. 9-9; Perth, Australia. 1987

[50] Ohsato H, Ohhashi T, Okuda T. Structure of $Ba_{6-3x}Sm_{8+2x}Ti_{18}O_{54}$ ($0<x<1$). In: Asian Crystallographic Association Conference (AsCA '92): Ext. Abstract 14U-50; November 1992; Singapore. 1992

[51] Kolar D, Gabrscek S, Suvorov D. Structural and dielectric properties of perovskite-like rare earth titanates. In: Duran P, Fernandes JF, editors. Third Euro-Ceramics V.2. Vol. 2. Spein: Faenza Editrice Lberica; 1993. pp. 229-234

[52] Lundberg M, Sundberg M, Magneli A. The "pentagonal column" as a building unit in crystal and defect structure of some groups of transition metal compounds. Journal of Solid State Chemistry. 1982;**44**:32-40

[53] Ohsato H, Nishigaki S, Okuda T. Superlattice and dielectric properties of dielectric compounds. Japanese Journal of Applied Physics. 1992;**31**(9B):3136-3138

[54] Ohsato H. Crystallography of dielectrics. In: Crystallography in Japan (II)–The glorious development. Tokyo, Japan: The Crystallographic Society of Japan; 2014. pp. 184-185 (Japanese)

[55] Ohsato H, Imaeda M, Komura A, Okuda T. Non-linear microwave quality factor change based on the site occupancy of cations on the tungstenbronze-type $Ba_{6-3x}R_{8+2x}Ti_{18}O_{54}$ (R = rare earth) solid solutions. In: Nair KM, Bhalla AS, editors. Dielectric Ceramic Materials, Ceramic Transactions 100. Hoboken, New Jersey: Wiley; 1998. pp. 41-50

[56] Ohsato H, Imaeda M, Takagi Y, Komura A, Okuda T. Microwave quality factor improved by ordering of Ba and rare-earth on the tungstenbronze-type $Ba_{6-3x}R_{8+2x}Ti_{18}O_{54}$ (R = La, Nd and Sm) solid solutions. In: Proceeding of the XIth IEEE International Symposium on Applications of Ferroelectrics; IEEE catalog number 98CH36245. 1998. pp. 509-512

[57] Ohsato H, Mizuta M, Okuda T. Crystal structure and microwave dielectric properties of Tungstenbronze-type $Ba_{6-3x}R_{8+2x}Ti_{18}O_{54}$ (R = La, Nd and Sm) solid solutions. In: Morawiec H, Stroz D, editors. Applied Crystallography. World Scientific Publishing; 1998. pp. 440-447

[58] Galasso F, Pyle J. Ordering in compounds of the $A(B'_{0.33}Ta_{0.67})O_3$ type. Inorganic Chemistry. 1963;**2**:482-484

[59] Yokotani Y, Tsuruta T, Okuyama K, Kugimiya K. Low-dielectric loss ceramics for microwave uses. National Technical Report. 1994;**40**:11-16 (Japanese)

[60] Tamura H, Konoike T, Sakabe Y, Wakino K. Microwave dielectric properties of Ba-Nd-Ti-O system doped with metal oxides. Journal of the American Ceramic Society. 1984;**67**:C-59

[61] Matsumoto H, Tamura H, Wakino K. $Ba(Mg,Ta)O_3$-$BaSnO_3$ high-Q dielectric resonator. Japanese Journal of Applied Physics. 1991;**30**:2347-2349

[62] Kageyama K. Crystal structure and microwave dielectric properties of $Ba(Zn_{1/3}Ta_{2/3})O_3$-$(Sr,Ba)(Ga_{1/3}Ta_{1/2})O_3$ ceramics. Journal of the American Ceramic Society. 1992;**75**:1767-1771

[63] Koga E, Moriwake H, Kakimoto K, Ohsato H. Synthesis of disordered $Ba(Zn_{1/3}Ta_{2/3})O_3$ by spark plasma sintering and its microwave Q factor. Japanese Journal of Applied Physics. 2006;**45**(9B):7484-7488

[64] Ohsato H, Azough F, Koga E, Kagomiya I, Kakimoto K, Freer R. High symmetry brings high Q instead of ordering in $Ba(Zn_{1/3}Nb_{2/3})O_3$: A HRTEM

study. In: Akedo J, Ohsato H, Shimada T, editors. Advances in Multifunctional Materials and Systems, Ceramic Transactions. Vol. 216. Hoboken, New Jersey: Wiley; 2010. pp. 129-136

[65] Wu H, Davies PK. Influence of non-stoichiometry on the structure and properties of $Ba(Zn_{1/3}Nb_{2/3})O_3$ microwave dielectrics: I. Substitution of $Ba_3W_2O_9$. Journal of the American Ceramic Society. 2006;**89**(7):2239-2249. DOI: 10.1111/j.1551-2916.2006.01007.x

[66] Surendran KP, Sebastian MT, Mohanan P, Moreira RL, Dias A. Effect of nonstoichiometry on the structure and microwave dielectric properties of $Ba(Mg_{0.33}Ta_{0.67})O_3$. Chemistry of Materials. 2005;**17**:142-151